

Dynamical Gauge Fields in Optomechanics

Stefan Walter¹ and Florian Marquardt^{1,2}

¹ *Institute for Theoretical Physics, University Erlangen-Nürnberg, Staudtstraße 7, 91058 Erlangen, Germany*

² *Max Planck Institute for the Science of Light, Günther-Scharowsky-Straße 1, 91058 Erlangen, Germany*

(Dated: October 26, 2015)

Artificial gauge fields for neutral particles such as photons, recently attracted a lot of attention in various fields ranging from photonic crystals to ultracold atoms in optical lattices to optomechanical arrays. Here we point out that, among all implementations of gauge fields, the optomechanical setting allows for the most natural extension where the gauge field becomes dynamical. The mechanical oscillation phases determine the effective artificial magnetic field for the photons, and once these phases are allowed to evolve, they respond to the flow of photons in the structure. We discuss a simple three-site model where we identify four different regimes of the gauge-field dynamics. Furthermore, we extend the discussion to a two-dimensional lattice. Our proposed scheme could for instance be implemented using optomechanical crystals.

PACS numbers: 42.50.Wk, 05.50.+q, 11.15.Kc

Introduction.— Gauge theories are very elementary concepts in physics. Today we know that the fundamental interactions between particles are mediated through gauge fields. The most common known gauge theory is classical electrodynamics which is described by Maxwell’s equations. In quantum mechanics the simplest but non trivial setting is a charged quantum particle moving in a classical externally prescribed electromagnetic background field giving rise to phenomena like the Aharonov-Bohm effect. Field theories such as quantum electrodynamics (QED) and quantum chromodynamics (QCD) are gauge theories where the gauge fields are dynamical in their own right and which interact with the matter fields, thereby mediating interactions among the matter particles. Recently, intriguing proposals showing how to synthesize dynamical gauge fields have been put forward. These proposals include the generation of Abelian as well as non-Abelian gauge fields realized with ultracold atoms in optical lattices [1–6] or with superconducting circuits [7, 8]. These settings can be viewed as a powerful tool for the quantum simulation of dynamical gauge theories such as QED and QCD on a lattice [9, 10].

In this article we study the most basic phonon-assisted photon tunneling process which is due to the optomechanical interaction. We are interested in the coupled photon-phonon dynamics and we show that in the optomechanical setting, phonons can act as a *dynamical* gauge field for photons. As we will show, in the optomechanical setting, these dynamical gauge fields arise in quite a natural manner.

In general, optomechanics describes the interaction of light and mechanical motion [11]. The prototypical optomechanical setting consists in a Fabry-Pérot cavity where one of the mirrors is free to oscillate. Due to the radiation pressure force the light inside the cavity interacts with the mirror’s motion. Tremendous experimental progress has been made during the last years, with achievements such as cooling a nanomechanical oscillator to its motional ground state [12, 13] and position measurements below the standard quantum limit [14], to name only a few examples. Mechanically and/or optically coupling several optomechanical systems leads to interesting

new physics. For instance, setups consisting of only a few optical and mechanical modes allow for nonreciprocal devices for photons [15–17]. Furthermore, larger optomechanical arrays, i.e., one- or two-dimensional arrangements of coupled optomechanical systems are promising candidate systems for studying many-body physics of photons or phonons [18–27]. Recently, it has been shown that optomechanical arrays also allow for the generation of artificial gauge fields for photons [26] and phonons [27]. The optomechanical implementation complements other proposals for generating artificial gauge fields for photons [28–36] and ultracold atoms in optical lattices [37–42].

As mentioned, *static* gauge fields for photons can also be realized using a variety of other methods, even though they are not necessarily as tunable as the optomechanical approach. In this article, however, we want to exploit a unique aspect of the optomechanical case that is not present in any of the other approaches that are based on geometry or externally applied periodic modulation. This is the fact that the mechanical vibrations (which generate the artificial gauge field) have oscillation phases that can evolve in response to the light field dynamics. Thus, our aim is to promote the static gauge fields to become dynamical gauge fields and investigate back-action effects of the dynamical gauge field on the hopping photons in the intriguing driven and dissipative setting of an optomechanical array. We introduce a simple model which gives rise to acoustical dynamical gauge fields for optical “matter” fields. To be more precise, we consider a photonic lattice (representing the matter fields) and artificial gauge fields (phonons) which can be attributed to directed links between two sites of the photonic lattice. Such a system could for instance be implemented in optomechanical crystal structures [43–48] or disk resonator arrays [49].

Model.— The crucial ingredient in our model is the phonon-assisted photon tunneling that can be generated by the optomechanical interaction: A photon a in a lattice hopping from site to site is accompanied by the coherent emission or absorption of a phonon b . For a photon tunneling between sites i and j , this is described by $b_{i,j}a_j^\dagger a_i$ (and the opposite

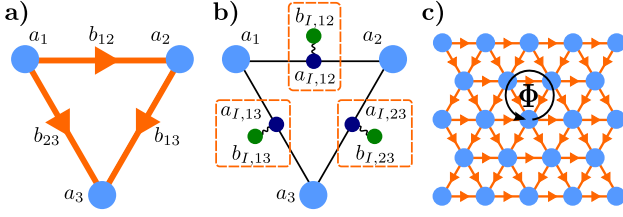


FIG. 1. (color online). a) Effective model for a three-site optomechanical implementation of dynamical gauge fields for photons a (light blue) coupling to phonons b (orange). Here, the optical frequencies increase around the triangle, $\nu_1 < \nu_2 < \nu_3$. As a consequence the links are directed, i.e., photons hopping in direction of the orange arrow absorb a phonon. b) Possible realization making use of the so-called “modulated link” scheme (see main text). Dark blue (green) dots depict the optical (mechanical) modes of the intermediate sites. Intermediate optical and mechanical modes couple optomechanically to form an optomechanical cell (dashed box). c) Two-dimensional triangular lattice. The arrows indicate the link direction.

process). Such a setting can be described by the Hamiltonian

$$H = \sum_j \nu_j a_j^\dagger a_j + \sum_l \omega_l b_l^\dagger b_l + \sum_l J_l b_l a_{l_2}^\dagger a_{l_1} + \text{H.c.} \quad (1)$$

We set $\hbar = 1$. Here, j denotes a lattice site, and $l = (l_1, l_2)$ is the index for a *directed* link from l_1 to l_2 . When a photon hops in the direction of the link, it absorbs a phonon. Photons (phonons) have frequencies ν_j (ω_l), and J_l are the coupling constants for the phonon-assisted photon tunneling process. For later use, we introduce the notation $b_{ij} = b_{ji}^\dagger$ and note that we use b_l and $b_{l_1 l_2}$ interchangeably. In Eq. (1) we made use of the rotating wave approximation which is valid for $\omega_l > \kappa, J_l$, where κ is the photon decay rate. As pointed out previously [26], non-reciprocity in photon transport can be engineered by introducing coherent inelastic transitions induced by mechanical vibrations. However, in contrast to Ref. [26] we will treat the vibrations as dynamical degrees of freedom, as explained below. Regardless of the details of the scheme, in order to make the inelastic processes resonant we need to ensure that the nearest neighbor on-site photon frequencies ν_j differ by the corresponding link phonon frequency ω_{ij} , i.e., $\omega_{ij} = \nu_j - \nu_i$, with the link direction from site i to j . This leads to *directed* links. Generally, a photon tunneling from a site with a low (high) on-site frequency to a site with a high (low) on-site frequency absorbs (emits) a phonon. Since the photons will eventually decay, we include the effects of dissipation and driving of the photons by adding a driving term $H_d = \sum_j E_j (a_j e^{i\omega_d t} + a_j^\dagger e^{-i\omega_d t})$ to the Hamiltonian (1) and by including dissipation of the photons at a rate κ (for details we refer to the Supplemental Material [50]).

This effective model can be realized in an optomechanical setting by building on the “modulated link” scheme that had been proposed in Ref. [26] to generate *static* artificial magnetic fields. We briefly review this scheme for one of

the links of the optomechanical setup depicted in Fig. 1 b). We explain why such a modulated link reduces to the link of the effective model of Eq. (1), cf. Fig. 1 a). The link between two optical modes i and j is realized with an intermediate optical mode $a_{I,l}$ which couples optomechanically to a mechanical mode $b_{I,l}$. Consequently, the link forms a single optomechanical cell. In the original “modulated link” scheme [26] the mechanical mode is externally driven into a large amplitude state $\langle b_{I,l}(t) \rangle = B_{I,l} e^{-i(\Omega_{I,l} t + \phi)}$ which leads to a modulation of the frequency of the intermediate optical mode $\omega_{I,j}(t) = \omega_{I,j} + 2g_0 B_{I,l} \cos(\Omega_{I,l} t + \phi)$, where g_0 is the single-photon optomechanical coupling strength. However, in contrast to [26], we will here assume the mechanical oscillator to be undergoing self-sustained optomechanical oscillations [11] instead of being externally driven. Thus it behaves as a limit-cycle oscillator with a fixed amplitude B and a free phase ϕ . In any case, in order to enable a photon to tunnel along such a link, the mechanical frequency has to match the difference of optical frequencies, as explained above. We note that other microscopic implementations are possible. For example, one might have a mechanical mode that directly couples to the hopping between optical modes, as has been worked out in detail for optomechanical crystals [51]. This would be connected to the “wavelength conversion scheme” discussed in Ref. [26].

Gauge field dynamics.— The corresponding equations of motion for the effective Hamiltonian (1) for the operators a_j and b_{ij} can be obtained using Heisenberg’s equations of motion. Here we will focus on the classical dynamics of the model, i.e., the limit of large coherent photon and phonon amplitudes. This is the most relevant regime for most of the current optomechanical setups (due to the small single-photon coupling strength g_0) [11]. Thus, we decompose the expectation values of the photon and phonon operators into a classical amplitude and a phase, $a_j = A_j e^{i\theta_j}$ and $b_{ij} = B_{ij} e^{i\phi_{ij}}$. From the full quantum Heisenberg equations of motion, the equations for the mechanical phases ϕ_{ij} become

$$\dot{\phi}_{ij} = -\omega_{ij} - \frac{J_{ij}}{B_{ij}} A_i A_j \cos(\phi_{ij} + \theta_{ij}), \quad (2)$$

where the link direction is from i to j , while the optical amplitudes A_i obey the following equations of motion

$$\dot{A}_i = -\sum_{j \neq i} J_{ij} B_{ij} \sin(\phi_{ij} + \theta_{ij}) A_j, \quad (3)$$

and the optical phases θ_i evolve according to

$$\dot{\theta}_i = -\nu_i - \sum_{j \neq i} J_{ij} B_{ij} \frac{A_j}{A_i} \cos(\phi_{ij} + \theta_{ij}). \quad (4)$$

Here and in the following we assume that the amplitudes of the limit-cycle oscillations $B_{ij} = B_{ji}$ are a constant of motion, i.e., $\dot{B}_{ij} = 0$. This regime can be reached by working with self-induced optomechanical oscillators (pumped by a blue-detuned laser) sufficiently above threshold [52]. Furthermore, we introduced $\theta_{jk} = \theta_j - \theta_k$ and used $\phi_{ij} = -\phi_{ji}$.

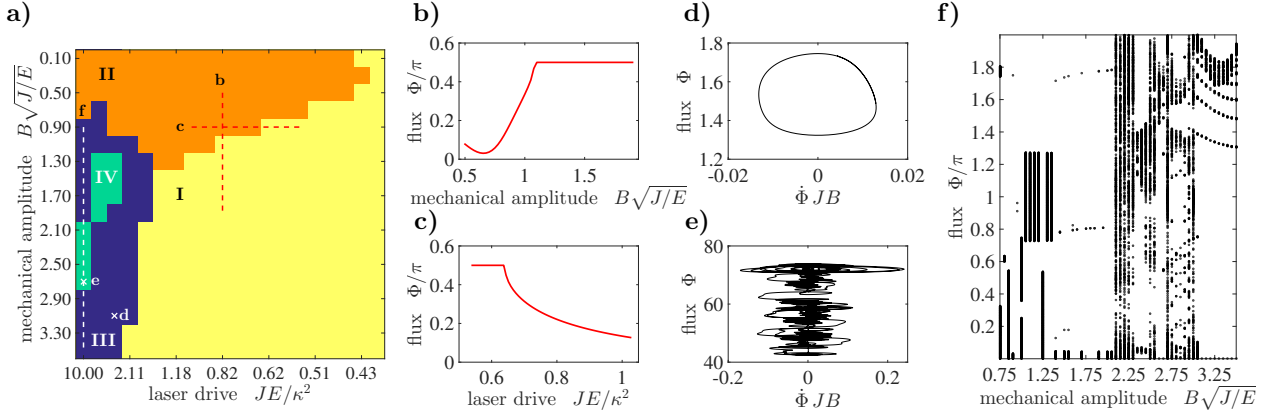


FIG. 2. (color online). a) Dynamical regimes of the flux Φ . Phase diagram as a function of mechanical amplitude and laser drive (which is resonant on site 1, $\omega_d = \nu_1$). We can distinguish four regimes for the flux dynamics. In regimes I and II the flux Φ is stationary and tends to a value equal to $\pi/2$ or different from it, respectively. In regimes III and IV the flux Φ is dynamical and can either show a periodic oscillatory or chaotic behavior, respectively. b) and c) Cuts along the red dashed lines in a) across the phase transition from regime I to II. d) and e) Two examples of phase space trajectories $\Phi(t) - \dot{\Phi}(t)$ in region III, where $\Phi(t)$ shows a periodic or chaotic behavior, respectively. f) Bifurcation diagram for the flux dynamics. We display the values of $\Phi(t)$ attained at the zero-crossings of $\dot{\Phi}(t)$. For the bifurcation diagram f) we used a higher resolution for values of $B\sqrt{J/E}$ than for the phase diagram a).

An important point we want to make at this stage is the invariance of the equations of motion under the following *local* $U(1)$ gauge transformation

$$\phi'_{ij} = \phi_{ij} + (\chi_j - \chi_i), \quad (5)$$

$$\theta'_i = \theta_i + \chi_i, \quad (6)$$

meaning that the observed evolution of the light *intensity* will not change, independent of the choice of χ_j . We assumed a static gauge choice χ ; otherwise Eqs. (5) and (6) would have to be supplemented by a change in frequencies: $\omega'_{ij} = \omega_{ij} + \dot{\chi}_i - \dot{\chi}_j$ and $\nu'_i = \nu_i - \dot{\chi}_i$.

We now ask under which conditions the gauge field will display nontrivial dynamics. It turns out that the time occurring in Eqs. (2), (3), and (4) can be rescaled by JB . After doing this, we observe that the entire dynamics only depends on the dimensionless ratio of A/B (where A is proportional to the laser drive amplitude). For the limit $A/B \rightarrow 0$, we expect that the oscillation phases (i.e., the magnetic field) will not be affected by the hopping photons, rather only defining a static magnetic field pattern. This can be seen from Eq. (2): for $A/B \ll 1$ the second term, which provides the coupling to the hopping photons, can be neglected. However, if A/B is large, we expect back-action of the hopping photons on the phonons leading to intriguing coupled dynamics of the gauge field.

Three-site model.— First, we will study the case of three sites. The resulting effective model for photons a_j on sites $j \in \{1, 2, 3\}$ and phonons b_l on links $l \in \{12, 23, 13\}$ is depicted in Fig. 1 a). Note that for three sites we define $a_4 = a_1$. For definiteness, we will assume $\nu_1 < \nu_2 < \nu_3$. For the present three-site model, the gauge freedom implies that only

the gauge invariant flux

$$\Phi = \phi_{13} + \phi_{21} + \phi_{32},$$

i.e., the sum of phases around the triangular plaquette, affects the dynamics of the photons. We want to mention that in the regime where the phonons are not influenced by the photons ($A/B \ll 1$ and consequently $\Phi = \text{const.}$) the Hamiltonian for the three-site model can be diagonalized and the setup can act (for $\Phi = \pm\pi/2$) as a photon circulator [30]. In the following we turn to the intriguing case where the photons interact with the phonons which produces a dynamical gauge field. Here, we discuss the driven and dissipative setting and furthermore choose equal tunneling amplitudes $J_l = J$ and mechanical amplitudes $B_l = B$. In the following we consider an example with a resonant drive on site $j = 1$ only, i.e., $E_1 = E$, $E_2 = E_3 = 0$ and $\omega_d = \nu_1$. As pointed out above, without drive and dissipation the dynamics only depends on the ratio A/B . As a consequence, the four parameters involved here, for the driven case (E, κ, B, J), can be combined into just two dimensionless parameters, $B\sqrt{J/E}$ and JE/κ^2 . The resulting “phase diagram” for the flux dynamics as a function of these two parameters is displayed in Fig. 2 a), and has been obtained from direct numerical simulations. These simulations reveal four distinct regimes. In regimes I and II the flux $\Phi(t)$ (after some transient behavior) approaches a stationary value of either $\Phi(t \rightarrow \infty) = \pi/2$ or different from it, respectively. In regimes III and IV, the flux $\Phi(t)$ is not stationary but shows a dynamical behavior even in the long-time limit of the driven and dissipative case. Most interestingly, the flux dynamics $\Phi(t)$ in this regime can either show periodic or chaotic behavior, region III and IV in Fig. 2 a), respectively. Figures 2 b) and c) show cuts along the red dashed lines marked in the phase diagram. The cuts indicate

a continuous phase transition from phase I to II. In Fig. 2 d) and e), we show two examples of the phase space $\Phi(t) - \dot{\Phi}(t)$ in regimes III and IV. Already at this level we can distinguish periodic [Fig. 2 d)] from chaotic [Fig. 2 e)] dynamics. A more involved characterization can be done with the help of a bifurcation diagram. To this end, we show the value of the flux $\Phi(t)$ evaluated at the zero crossings of $\dot{\Phi}(t)$, in the long-time limit, as a function of the mechanical amplitude B in Fig. 2 f). This bifurcation diagram allows us to distinguish the periodic [region III in Fig. 2 a)] from the chaotic [region IV in Fig. 2 a)] flux dynamics within the whole phase diagram for $\Phi(t)$. Analytical progress can be made in the limit where the photon dynamics is much faster than the phonon dynamics. We are then able to apply a Born-Oppenheimer approximation and adiabatically eliminate the photons. To be more precise, we solve $da_i/dt = 0$ where

$$\dot{a}_j = \left[-i(\nu_j - \omega_d) - \frac{\kappa}{2} \right] a_j - iE_j - iJB \sum_{k \neq j} e^{-i\phi_{jk}} a_k,$$

and use this instantaneous solution to eliminate a_i from the equations of motion for the mechanical phases ϕ_{ij} (for details we refer to the Supplemental Material [50]). In the case of a resonant ($\omega_d = \nu_1$) drive on site $j = 1$, this approximation leads to the following equation of motion for the flux:

$$\dot{\Phi} = \frac{16E^2}{JB^3} \frac{(4 + \frac{\kappa^2}{J^2 B^2}) \cos(\Phi)}{\frac{\kappa^2}{J^2 B^2} [12 + \frac{\kappa^2}{J^2 B^2}]^2 + [16 \cos(\Phi)]^2}. \quad (7)$$

From Eq. (7) we find $\Phi(t \rightarrow \infty) = \pi/2$ which shows very good agreement with the exact numerical long-time dynamics in regime I. This approach fails to reproduce the flux dynamics $\Phi(t)$ in the other two regimes since there we are not able to adiabatically eliminate the photons. We also want to mention that both $\Phi = +\pi/2$ and $\Phi = -\pi/2$ are fixed points of Eq. (7). It turns out that for a resonant drive on site $j = 1$, $\Phi = -\pi/2$ is an unstable fixed point of Eq. (7). The asymmetry between $+\pi/2$ and $-\pi/2$ is due to the breaking of translational invariance, necessarily produced by the link directions. In contrast, a resonant drive on site $j = 2(3)$ would have $\Phi = -\pi/2(+\pi/2)$ as a stable fixed point.

Lattices.— We extend the three-site model to two-dimensional lattices and illustrate the dynamical behaviour on a triangular lattice [Fig. 1 c)]. We focus on a driven and dissipative situation. Going from three sites to a lattice, a significant new feature comes into play: the artificial dynamical magnetic field produced by the phonons can now exert a Lorentz force that bends the path of any light-beam propagating in the two-dimensional array. Therefore, we end up with a dynamical interplay where the flow of the photons changes the spatial distribution of the magnetic flux density which then acts back on the dynamics of the light field. In the following we assume equal mechanical amplitudes $B_l = B$ and tunneling amplitudes $J_l = J$. The frequencies of the optical modes determine the link directions. We choose a scenario with the link directions as depicted in Fig. 1 c), cf. Supplemental Material [50] for details. We note that this is not the only possible

choice. In fact the intricate photon and phonon dynamics depends on the link pattern. We illustrate the nonlinear structure formation in this model for the case of having only a single site illuminated by a laser. In Fig. 3 we show the temporal evolu-

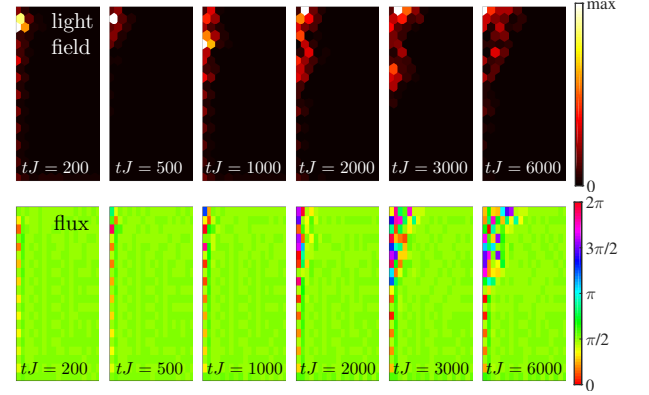


FIG. 3. (color online). Evolution of the light field on a lattice with a dynamical gauge field of vibrational origin. We show the light intensity $|A_{i,j}|^2$ on each site (top row) and flux Φ per plaquette (bottom row) at different times. The simulation was carried out on a 21×21 triangular lattice, whose left half is shown here. The resonant drive is on the site on the corner and the initial flux per plaquette is $\Phi = \pi/2$. No steady state of either photons or phonons is reached. We chose $B\sqrt{J/E} = 3.16$, $JE/\kappa^2 = 10$.

tion of the light intensity (top row) as well as the magnetic field (bottom row) on the lattice. At first the photons experience a static magnetic field which is set by the initial phases of the mechanical oscillations (here chosen such that the initial flux is $\Phi = \pi/2$) and start to move along the edge. Due to the back-action of the photons (which primarily move along the edge) on the phonons, the flux per plaquette changes. This in turn leads to a reconfiguration of the magnetic field. Even though the photons live only for a short time $1/\kappa$ before escaping the structure, the system develops a spatial “memory” in the form of the mechanical oscillation phases, where previous photons leave their imprint. The photons then react to this new magnetic field configuration. In this specific example, the photons reverse their direction of motion. In the simulations performed here, the system does not reach a steady state in the long-time limit. Collective behavior such as synchronization and pattern formation of mechanical limit-cycle oscillators have recently been theoretically studied in optomechanical arrays [53–55]. In connection to these investigations, further studies on gauge field dynamics in optomechanics could for instance address questions on synchronization and possible dynamical pattern formation of the magnetic field.

Conclusion.— We have shown that dynamical gauge fields in optomechanical arrays arise quite naturally. The evolving mechanical phases, which respond to the flow of the photons, represent a dynamical gauge field for the latter. Already the three-site model shows intriguing dynamics which leads to a rather complex phase diagram for the flux dynamics. With experiments pushing towards multi-mode optomechanical se-

tups, the three-site model seems feasible to be realized in the near future and would pave the way for further studies of dynamical gauge fields in optomechanical arrays.

Acknowledgements: We acknowledge helpful discussions with Roland Lauter, and thank Vittorio Peano and Talitha Weiss for a careful reading of the manuscript. This work was financially supported by the Marie Curie ITN cQOM and the ERC OPTOMECH.

-
- [1] K. Osterloh, M. Baig, L. Santos, P. Zoller, and M. Lewenstein, Phys. Rev. Lett. **95**, 010403 (2005).
 - [2] J. Ruseckas, G. Juzelinis, P. Öhberg, and M. Fleischhauer, Phys. Rev. Lett. **95**, 010404 (2005).
 - [3] P. Hauke, O. Tieleman, A. Celi, C. Ölschläger, J. Simonet, J. Struck, M. Weinberg, P. Windpassinger, K. Sengstock, M. Lewenstein, and A. Eckardt, Phys. Rev. Lett. **109**, 145301 (2012).
 - [4] D. Banerjee, M. Dalmonte, M. Müller, E. Rico, P. Stebler, U. J. Wiese, and P. Zoller, Phys. Rev. Lett. **109**, 175302 (2012).
 - [5] E. Zohar, J. I. Cirac, and B. Reznik, Phys. Rev. A **88**, 023617 (2013).
 - [6] M. J. Edmonds, M. Valiente, G. Juzelinis, L. Santos, and P. Öhberg, Phys. Rev. Lett. **110**, 085301 (2013).
 - [7] D. Marcos, P. Rabl, E. Rico, and P. Zoller, Phys. Rev. Lett. **111**, 110504 (2013).
 - [8] D. Marcos, P. Widmer, E. Rico, M. Hafezi, P. Rabl, U. J. Wiese, and P. Zoller, Annals of Physics **351**, 634 (2014).
 - [9] U. J. Wiese, Ann. der Phys. **525**, 777 (2013).
 - [10] E. Zohar, J. I. Cirac, and B. Reznik, arXiv:1503.02312 (2015).
 - [11] M. Aspelmeyer, T. J. Kippenberg, and F. Marquardt, Rev. Mod. Phys. **86**, 1391 (2014).
 - [12] J. D. Teufel, T. Donner, D. Li, J. W. Harlow, M. S. Allman, K. Cicak, A. J. Sirois, J. D. Whittaker, K. W. Lehnert, and R. W. Simmonds, Nature **475**, 359 (2011).
 - [13] J. Chan, T. P. Mayer Alegre, A. H. Safavi-Naeini, J. T. Hill, A. Krause, S. Gröblacher, M. Aspelmeyer, and O. Painter, Nature **478**, 89 (2011).
 - [14] J. D. Teufel, T. Donner, M. A. Castellanos-Beltran, J. W. Harlow, and K. W. Lehnert, Nat. Nanotechnol. **4**, 820 (2009).
 - [15] S. Manipatruni, J. T. Robinson, and M. Lipson, Phys. Rev. Lett. **102**, 213903 (2009).
 - [16] S. J. M. Habraken, K. Stannigel, M. D. Lukin, P. Zoller, and P. Rabl, New J. Phys. **14**, 115004 (2012).
 - [17] M. Hafezi and P. Rabl, Opt. Express **20**, 7672 (2012).
 - [18] M. Bhattacharya and P. Meystre, Phys. Rev. A **78**, 041801 (2008).
 - [19] D. E. Chang, A. H. Safavi-Naeini, M. Hafezi, and O. Painter, New J. Phys. **13**, 023003 (2011).
 - [20] A. Xuereb, C. Genes, and A. Dantan, Phys. Rev. Lett. **109**, 223601 (2012).
 - [21] A. Tomadin, S. Diehl, M. D. Lukin, P. Rabl, and P. Zoller, Phys. Rev. A **86**, 033821 (2012).
 - [22] M. Schmidt, M. Ludwig, and F. Marquardt, New J. Phys. **14**, 125005 (2012).
 - [23] U. Akram, W. Munro, K. Nemoto, and G. J. Milburn, Phys. Rev. A **86**, 042306 (2012).
 - [24] W. Chen and A. A. Clerk, Phys. Rev. A **89**, 033854 (2014).
 - [25] M. Schmidt, V. Peano, and F. Marquardt, New J. Phys. **17**, 023025 (2015).
 - [26] M. Schmidt, S. Keßler, V. Peano, O. Painter, and F. Marquardt, Optica **2**, 635 (2015).
 - [27] V. Peano, C. Brendel, M. Schmidt, and F. Marquardt, Phys. Rev. X **5**, 031011 (2015).
 - [28] S. Raghu and F. D. M. Haldane, Phys. Rev. Lett. **100**, 013904 (2008).
 - [29] Z. Wang, Y. Chong, J. D. Joannopoulos, and M. Soljačić, Nature **461**, 772 (2009).
 - [30] J. Koch, A. a. Houck, K. Le Hur, and S. M. Girvin, Phys. Rev. A **82**, 043811 (2010).
 - [31] R. O. Umucallar and I. Carusotto, Phys. Rev. A **84**, 043804 (2011).
 - [32] M. Hafezi, E. A. Demler, M. D. Lukin, and J. M. Taylor, Nat. Phys. **7**, 907 (2011).
 - [33] K. Fang, Z. Yu, and S. Fan, Nature Photon. **6**, 782 (2012).
 - [34] L. Lu, J. D. Joannopoulos, and M. Soljačić, Nature Photon. **8**, 821 (2014).
 - [35] M. Hafezi, S. Mittal, J. Fan, A. Migdall, and J. M. Taylor, Nature Photon. **7**, 1001 (2013).
 - [36] S. Mittal, J. Fan, S. Faez, A. Migdall, J. M. Taylor, and M. Hafezi, Phys. Rev. Lett. **113**, 087403 (2014).
 - [37] D. Jaksch and P. Zoller, New J. Phys. **5**, 56 (2003).
 - [38] A. S. Sørensen, E. Demler, and M. D. Lukin, Phys. Rev. Lett. **94**, 086803 (2005).
 - [39] Y. J. Lin, R. L. Compton, K. Jiménez-García, J. V. Porto, and I. B. Spielman, Nature **462**, 628 (2009).
 - [40] M. Aidelsburger, M. Atala, S. Nascimbène, S. Trotzky, Y. A. Chen, and I. Bloch, Phys. Rev. Lett. **107**, 255301 (2011).
 - [41] M. Aidelsburger, M. Atala, M. Lohse, J. T. Barreiro, B. Paredes, and I. Bloch, Phys. Rev. Lett. **111**, 185301 (2013).
 - [42] G. Jotzu, M. Messer, R. Desbuquois, M. Lebrat, T. Uehlinger, D. Greif, and T. Esslinger, Nature **515**, 237 (2014).
 - [43] M. Eichenfield, J. Chan, R. M. Camacho, K. J. Vahala, and O. Painter, Nature **462**, 78 (2009).
 - [44] A. H. Safavi-Naeini and O. Painter, Opt. Express **18**, 14926 (2010).
 - [45] A. H. Safavi-Naeini, T. P. Mayer Alegre, M. Winger, and O. Painter, Appl. Phys. Lett. **97**, 181106 (2010).
 - [46] E. Gavartin, R. Braive, I. Sagnes, O. Arcizet, A. Beveratos, T. J. Kippenberg, and I. Robert-Philip, Phys. Rev. Lett. **106**, 203902 (2011).
 - [47] J. Chan, T. P. Mayer Alegre, A. H. Safavi-Naeini, J. T. Hill, A. Krause, S. Gröblacher, M. Aspelmeyer, and O. Painter, Nature **478**, 89 (2011).
 - [48] A. H. Safavi-Naeini, J. T. Hill, S. Meenehan, J. Chan, S. Gröblacher, and O. Painter, Phys. Rev. Lett. **112**, 153603 (2014).
 - [49] M. Zhang, S. Shah, J. Cardenas, and M. Lipson, arXiv:1505.02009 (2015).
 - [50] See Supplemental Material at [link] for details.
 - [51] A. H. Safavi-Naeini and O. Painter, New J. Phys. **13**, 013017 (2011).
 - [52] F. Marquardt, J. G. E. Harris, and S. M. Girvin, Phys. Rev. Lett. **96**, 103901 (2006).
 - [53] G. Heinrich, M. Ludwig, J. Qian, B. Kubala, and F. Marquardt, Phys. Rev. Lett. **107**, 043603 (2011).
 - [54] M. Ludwig and F. Marquardt, Phys. Rev. Lett. **111**, 073603 (2013).
 - [55] R. Lauter, C. Brendel, S. J. M. Habraken, and F. Marquardt, Phys. Rev. E **92**, 012902 (2015).

Supplemental Material for “Dynamical Gauge Fields in Optomechanics”

Stefan Walter ¹ and Florian Marquardt ^{1,2}

¹ *Institute for Theoretical Physics, University Erlangen-Nürnberg, Staudtstraße 7, 91058 Erlangen, Germany*

² *Max Planck Institute for the Science of Light, Günther-Scharowsky-Straße 1, 91058 Erlangen, Germany*

THE THREE-SITE MODEL: DIAGONALIZATION

Here, we give some further details on the three-site model given by Eq. (1) of the main text which in its explicit form reads

$$H = \sum_{j \in \{1,2,3\}} \nu_j a_j^\dagger a_j + \sum_{l \in \{12,23,13\}} \omega_l b_l^\dagger b_l + J_{12} \left(b_{12} a_2^\dagger a_1 + \text{H.c.} \right) + J_{23} \left(b_{23} a_3^\dagger a_2 + \text{H.c.} \right) + J_{13} \left(b_{13} a_1^\dagger a_3 + \text{H.c.} \right). \quad (\text{S1})$$

The equations of motion are obtained straight forwardly by using Heisenberg’s equation of motion. The mechanical phases ϕ_{ij} evolve according to

$$\begin{aligned} \dot{\phi}_{12} &= -\omega_{12} - \frac{J_{12}}{B_{12}} A_1 A_2 \cos(\phi_{12} + \theta_{12}), \\ \dot{\phi}_{23} &= -\omega_{23} - \frac{J_{23}}{B_{23}} A_2 A_3 \cos(\phi_{23} + \theta_{23}), \\ \dot{\phi}_{13} &= -\omega_{13} - \frac{J_{13}}{B_{13}} A_1 A_3 \cos(\phi_{13} + \theta_{13}). \end{aligned}$$

The optical amplitudes A_j obey the following equations of motion

$$\begin{aligned} \dot{A}_1 &= -J_{12} B_{12} \sin(\phi_{12} + \theta_{12}) A_2 - J_{13} B_{13} \sin(\phi_{13} + \theta_{13}) A_3, \\ \dot{A}_2 &= +J_{12} B_{12} \sin(\phi_{12} + \theta_{12}) A_1 - J_{23} B_{23} \sin(\phi_{23} + \theta_{23}) A_3, \\ \dot{A}_3 &= +J_{13} B_{13} \sin(\phi_{13} + \theta_{13}) A_1 + J_{23} B_{23} \sin(\phi_{23} + \theta_{23}) A_2, \end{aligned}$$

and the optical phases θ_j

$$\begin{aligned} \dot{\theta}_1 &= -\nu_1 - J_{12} B_{12} \frac{A_2}{A_1} \cos(\phi_{12} + \theta_{12}) - J_{13} B_{13} \frac{A_3}{A_1} \cos(\phi_{13} + \theta_{13}), \\ \dot{\theta}_2 &= -\nu_2 - J_{12} B_{12} \frac{A_1}{A_2} \cos(\phi_{12} + \theta_{12}) - J_{23} B_{23} \frac{A_3}{A_2} \cos(\phi_{23} + \theta_{23}), \\ \dot{\theta}_3 &= -\nu_3 - J_{23} B_{23} \frac{A_2}{A_3} \cos(\phi_{23} + \theta_{23}) - J_{13} B_{13} \frac{A_1}{A_3} \cos(\phi_{13} + \theta_{13}). \end{aligned}$$

As mentioned in the main text, for $A/B \ll 1$, i.e., in the case of a static flux Φ , and for $\Phi = \pm\pi/2$ a circulator behavior is expected, cf. Ref. [30]. A solution to this system of coupled first order differential equations with initially one photon on site 1 and a phase $\Phi = -\pi/2$ is shown in Fig. S1 a) and b), where the circulator behavior is clearly visible, i.e., the photon is moving counterclockwise around the triangular plaquette.

The Hamiltonian of the three-site model can be diagonalized best after going into a rotating frame by applying the transformation

$$U = e^{it \sum_j \nu_j a_j^\dagger a_j} e^{it \sum_l \omega_l b_l^\dagger b_l},$$

to Eq. (S1) which leads to the Hamiltonian

$$H = J_{12} B_{12} \left(e^{-i\phi_{12}} a_1^\dagger a_2 + \text{H.c.} \right) + J_{23} B_{23} \left(e^{-i\phi_{23}} a_2^\dagger a_3 + \text{H.c.} \right) + J_{13} B_{13} \left(e^{i\phi_{13}} a_3^\dagger a_1 + \text{H.c.} \right).$$

Since we are here interested in the eigenvalues, we can perform a gauge transform $a_j \rightarrow a_j e^{i\chi_j}$ and make the following gauge choice

$$\begin{aligned} -\phi_{12} + \chi_2 - \chi_1 &= \tilde{\Phi}, \\ -\phi_{23} + \chi_3 - \chi_2 &= \tilde{\Phi}, \\ \phi_{13} + \chi_1 - \chi_3 &= \tilde{\Phi}, \end{aligned}$$

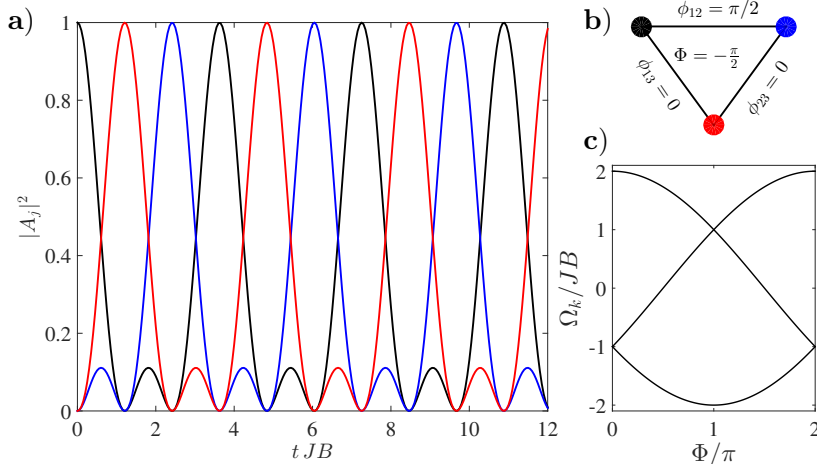


FIG. S1. (color online). a) Optical amplitudes $|A_j|^2$. The initial state has one photon on site 1. For $\Phi = -\pi/2$, the initial excitation moves counterclockwise around the triangular plaquette shown in b). For $\Phi = \pi/2$, the initial excitation would move clockwise around the triangle. c) Dispersion relation Ω_k as a function of the phase Φ .

which we can write as $\phi_{13} - \phi_{12} - \phi_{23} = 3\tilde{\Phi} = \Phi$. The Hamiltonian can then be written as

$$H = \sum_{j=1}^3 J_j B_j e^{i\tilde{\Phi}} a_j^\dagger a_{j+1} + \text{H.c.},$$

where we assumed periodic boundary conditions, i.e., $a_4 = a_1$ and for convenience we introduce $J_{12,23,13} \rightarrow J_{1,2,3}$ and similarly for $B_{12,23,13}$. By introducing normal modes

$$a_j^\dagger = \frac{1}{\sqrt{3}} \sum_{k=0}^2 e^{-2\pi i k j / 3} A_k^\dagger,$$

$$A_k^\dagger = \frac{1}{\sqrt{3}} \sum_{j=1}^3 e^{2\pi i k j / 3} a_j^\dagger,$$

and furthermore assuming equal tunneling amplitude J and limit-cycle amplitude B , the Hamiltonian can be diagonalized

$$H = \sum_{k=0}^2 \Omega_k A_k^\dagger A_k, \quad (1)$$

where $\Omega_k = 2JB \cos(\tilde{\Phi} + 2\pi k/3)$. As already pointed out in Ref. [30], for $\Phi = \pm\pi/2$ this setup shows the behaviour of a photon circulator.

THE THREE-SITE MODEL: INCLUDING DRIVE AND DISSIPATION

Since the photons eventually decay, we add photon loss and drive to the system. This is best done starting with the Hamiltonian (S1) and adding a driving term $H_d = \sum_{j \in \{1,2,3\}} E_j (a_j e^{i\omega_d t} + a_j^\dagger e^{-i\omega_d t})$. Going into a frame rotating with the driving frequency ω_d , we obtain

$$H = \sum_{j \in \{1,2,3\}} (\nu_j - \omega_d) a_j^\dagger a_j + \sum_{j \in \{1,2,3\}} E_j (a_j + a_j^\dagger) + \sum_{l \in \{12,23,13\}} \omega_l b_l^\dagger b_l$$

$$+ J_{12} B_{12} (e^{-i\phi_{12}} a_1^\dagger a_2 + \text{H.c.}) + J_{23} B_{23} (e^{-i\phi_{23}} a_2^\dagger a_3 + \text{H.c.}) + J_{13} B_{13} (e^{i\phi_{13}} a_3^\dagger a_1 + \text{H.c.}).$$

Including dissipation of the photons at a rate κ and neglecting effects due to quantum noise, the equations of motion for the photons become $d\vec{a}/dt = -iM\vec{a} - i\vec{E}$ with

$$\begin{aligned}\vec{a} &= (a_1, a_2, a_3)^T, \\ \vec{E} &= (E_1, E_2, E_3)^T, \\ M &= \begin{pmatrix} (\nu_1 - \omega_d) - i\frac{\kappa}{2} & J_{12}B_{12}e^{-i\phi_{12}} & J_{13}B_{13}e^{-i\phi_{13}} \\ J_{12}B_{12}e^{i\phi_{12}} & (\nu_2 - \omega_d) - i\frac{\kappa}{2} & J_{23}B_{23}e^{-i\phi_{23}} \\ J_{13}B_{13}e^{i\phi_{13}} & J_{23}B_{23}e^{i\phi_{23}} & (\nu_3 - \omega_d) - i\frac{\kappa}{2} \end{pmatrix}.\end{aligned}$$

The equations of motion for the phases ϕ_{ij} are unchanged. In Fig. S2 we show the optical amplitude $|\langle a_j \rangle|^2 = |A_j|^2$ as a function of the flux Φ and the drive frequency ω_d . Figure S2 almost resembles the eigenfrequencies Ω_k in Fig. S1 c) which we obtained from diagonalizing the Hamiltonian.

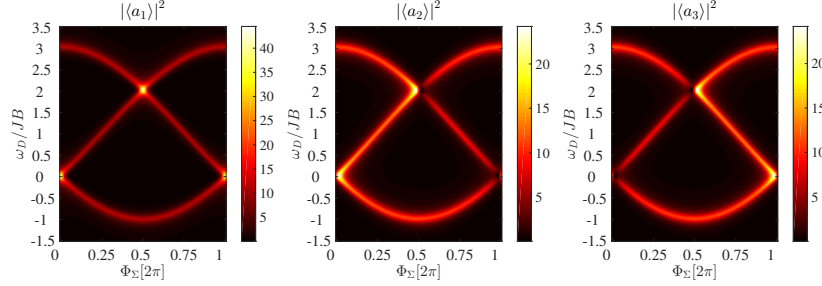


FIG. S2. (color online). Left: $|A_1|^2$. Middle: $|A_2|^2$. Right: $|A_3|^2$. Here we only drive site $j = 1$, i.e., $E_1 = E, E_2 = E_3 = 0$ and choose $JE/\kappa^2 = 0.025$, and $B\sqrt{J/E} = 31.6$.

THE TRIANGULAR LATTICE: EQUATIONS OF MOTION

On a two-dimensional triangular lattice we denote dynamical variables on lattice site n, m with a subscripts (n, m) and dynamical variables on the directed links from site n, m to site k, l by a subscript $(n, m)(k, l)$. The equations of motion for the mechanical phases $\phi_{(n, m)(n, m+1)}$ on the lattice links are

$$\begin{aligned}\dot{\phi}_{(n, m)(n, m+1)} &= -\omega_{(n, m)(n, m+1)} - \frac{J_{(n, m)(n, m+1)}}{B_{(n, m)(n, m+1)}} A_{n, m} A_{n, m+1} \cos(\phi_{(n, m)(n, m+1)} + \theta_{n, m} - \theta_{n, m+1}), \\ \dot{\phi}_{(n, m+1)(n+1, m)} &= -\omega_{(n, m+1)(n+1, m)} - \frac{J_{(n, m+1)(n+1, m)}}{B_{(n, m+1)(n+1, m)}} A_{n, m+1} A_{n+1, m} \cos(\phi_{(n, m+1)(n+1, m)} + \theta_{n, m+1} - \theta_{n+1, m}), \\ \dot{\phi}_{(n, m)(n+1, m)} &= -\omega_{(n, m)(n+1, m)} - \frac{J_{(n, m)(n+1, m)}}{B_{(n, m)(n+1, m)}} A_{n, m} A_{n+1, m} \cos(\phi_{(n, m)(n+1, m)} + \theta_{n, m} - \theta_{n+1, m}).\end{aligned}$$

The optical amplitudes $A_{n, m}$ obey the equations of motion

$$\begin{aligned}\dot{A}_{n, m} &= -J_{(n, m)(n, m+1)} B_{(n, m)(n, m+1)} \sin(\phi_{(n, m)(n, m+1)} + \theta_{n, m} - \theta_{n, m+1}) A_{n, m+1} \\ &\quad - J_{(n, m)(n+1, m)} B_{(n, m)(n+1, m)} \sin(\phi_{(n, m)(n+1, m)} + \theta_{n, m} - \theta_{n+1, m}) A_{n+1, m} \\ &\quad + J_{(n, m-1)(n, m)} B_{(n, m-1)(n, m)} \sin(\phi_{(n, m-1)(n, m)} + \theta_{n, m-1} - \theta_{n, m}) A_{n, m-1} \\ &\quad - J_{(n, m)(n+1, m-1)} B_{(n, m)(n+1, m-1)} \sin(\phi_{(n, m)(n+1, m-1)} + \theta_{n, m} - \theta_{n+1, m-1}) A_{n+1, m-1} \\ &\quad + J_{(n-1, m)(n, m)} B_{(n-1, m)(n, m)} \sin(\phi_{(n-1, m)(n, m)} + \theta_{n-1, m} - \theta_{n, m}) A_{n-1, m} \\ &\quad + J_{(n-1, m+1)(n, m)} B_{(n-1, m+1)(n, m)} \sin(\phi_{(n-1, m+1)(n, m)} + \theta_{n-1, m+1} - \theta_{n, m}) A_{n-1, m+1},\end{aligned}$$

and the optical phases $\theta_{n,m}$ on a lattice site evolve according to

$$\begin{aligned}
\dot{\theta}_{n,m} = & -\nu_{n,m} \\
& - J_{(n,m)(n,m+1)} B_{(n,m)(n,m+1)} \frac{A_{n,m+1}}{A_{n,m}} \cos(\phi_{(n,m)(n,m+1)} + \theta_{n,m} - \theta_{n,m+1}) \\
& - J_{(n,m)(n+1,m)} B_{(n,m)(n+1,m)} \frac{A_{n+1,m}}{A_{n,m}} \cos(\phi_{(n,m)(n+1,m)} + \theta_{n,m} - \theta_{n+1,m}) \\
& - J_{(n,m-1)(n,m)} B_{(n,m-1)(n,m)} \frac{A_{n,m-1}}{A_{n,m}} \cos(\phi_{(n,m-1)(n,m)} + \theta_{n,m-1} - \theta_{n,m}) \\
& - J_{(n,m)(n+1,m-1)} B_{(n,m)(n+1,m-1)} \frac{A_{n+1,m-1}}{A_{n,m}} \cos(\phi_{(n,m)(n+1,m-1)} + \theta_{n,m} - \theta_{n+1,m-1}) \\
& - J_{(n,m)(n+1,m+1)} B_{(n,m)(n+1,m+1)} \frac{A_{n+1,m+1}}{A_{n,m}} \cos(\phi_{(n,m)(n+1,m+1)} + \theta_{n,m} - \theta_{n+1,m+1}) \\
& - J_{(n-1,m+1)(n,m)} B_{(n-1,m+1)(n,m)} \frac{A_{n-1,m+1}}{A_{n,m}} \cos(\phi_{(n-1,m+1)(n,m)} + \theta_{n-1,m+1} - \theta_{n,m}).
\end{aligned}$$

A driving term on a particular site and dissipation of the photons on each site can be added straightforwardly, as also done for the three-site model.

THE TRIANGULAR LATTICE: DISTRIBUTION OF OPTICAL AND MECHANICAL FREQUENCIES

As mentioned in the main text, the links are directed: A photon tunneling from a site with a low (high) on-site frequency to a site with a high (low) on-site frequency absorbs (emits) a phonon. These processes have to be resonant which could be achieved by distributing the photon and phonon frequencies in the right way. For instance, the frequencies can be arranged as shown in Fig. S3.

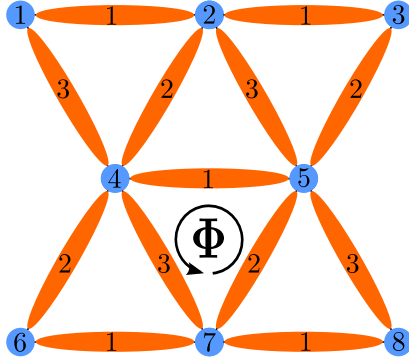


FIG. S3. (color online). Possible distribution of optical (blue dots) and mechanical (orange ellipses) frequencies on a 3×3 triangular lattice as an example.